Statistical Distribution of the Layered Rough Surface Index (LRSI)

Richard Dusséaux, Saddek Afifi

Progress In Electromagnetics Research C, Vol. 94, 75–87, 2019

Statistical Distribution of the Layered Rough Surface Index (LRSI)

Richard Dusséaux[1, *] and Saddek Afifi[2]

Abstract—In this paper we determine the statistical distributions of the co- and cross-polarized Layered Rough Surface Index (LRSI) for three-dimensional layered structures with an arbitrary number of slightly rough interfaces illuminated by an electromagnetic plane wave. For infinite surface areas and Gaussian centered height distributions, we show within the framework of the first-order small perturbation method that the LRSI under a given observation direction is a random variable, whose statistical distribution is only function of two parameters. Contrary to the intensity ratio which follows a heavy-tailed distribution, the LRSI has finite mean and variance. For a structure air/clayey soil/rock, we analyze the influence of a snow layer upon the probability laws in the cases of Gaussian or exponential correlation functions.

1. INTRODUCTION

In [1], we established the closed-formulae for the probability density function (PDF) of the co- and cross-polarized intensity ratio in any observation direction for the field scattered from three-dimensional layered structures with an arbitrary number of rough interfaces under an illumination by an electromagnetic plane wave. Calculations were carried out within the framework of the first-order small perturbation method and assumed slightly rough boundaries with infinite surface areas and Gaussian centered height distributions [2–7]. The interfaces were correlated or not, isotropic or not, but the spectra and cross-spectra were Gaussian. We have demonstrated that the PDF is fully defined by two parameters that depend on the second-order statistical moments of the real and imaginary parts of scattering amplitudes [8–11]. But, the co- and cross-polarized intensity ratios under an observation direction are non-negative real-valued random variables which follow heavy-tailed distributions and do not have a finite mean and a finite variance.

The co- and cross-polarized intensity ratios are important discriminators in the study of polarimetric and interferometric data. The normalized difference polarization index is defined as the ratio $(I_{(ba)} - I_{(b'a')})/(I_{(ba)} + I_{(b'a')})$ where the quantities $I_{(ba)}$ and $I_{(b'a')}$ designate the (b)- and (b')-polarized component of the scattered intensity under the (a)- and (a')-polarized incident wave, respectively. This descriptor is often used for labelling of different land cover types [12, 13].

In the present paper, we extend the work conducted in [1] and determine the closed-form expression for the PDF of the Layered Rough Surface Index. The LRSI associated with the components (ba) and $(b'a')$ of the scattered wave is defined as the ratio $I_{(b'a')}/(I_{(ba)} + I_{(b'a')})$. For a given direction, this descriptor is a random variable defined over $[0, +1]$ with a finite mean and a finite variance. We also establish the analytical expression of the Cumulative Density Function of the LRSI as well as those of its mean and its variance. To our knowledge, it is the first time that the properties of this indicator are found.

Received 22 March 2019, Accepted 24 June 2019, Scheduled 13 July 2019
* Corresponding author: Richard Dusséaux (richard.dusseaux@latmos.ipsl.fr).
[1] Université de Versailles Saint-Quentin en Yvelines/Paris-Saclay, LATMOS/IPSL/CNRS, 11 Boulevard d'Alembert, Guyancourt 78280, France. [2] Laboratoire de Physique des Lasers, de Spectroscopie Optique et d'Opto-électronique (LAPLASO), Badji Mokhtar-Annaba University, Annaba 23000, Algeria.

The Canopy Structure Index (CSI) extracted from polarimetric data is often used for analysing the relative presence of vertical scatterers (trunks and stems) of vegetation [14, 15]. This indicator is defined by the same formula as the LRSI but from the average intensities. In the present paper, for a structure air/clayey soil/rock, we analyze the influence of a snow layer upon the probability laws for Gaussian and exponential correlation functions.

This paper is organized as follows. In Section 2, we present the statistical properties of the three-dimensional layered structure under consideration and define the interface spectra and their cross-spectra for Gaussian and exponential correlation functions with or without anisotropy. In Section 3, within the framework of the first-order SPM, we give expressions for the co- and cross-polarized scattering amplitudes and for the scattered intensities. In Section 4, we establish in any observation plane the closed-form expressions for the distribution of the LRSI. Section 5 is devoted to the study of probability laws for a stratification air/clayey soil/rock with or without snow cover.

2. STATISTICAL DESCRIPTION OF INTERFACES

Consider the three-dimensional N-layer homogeneous dielectric structure shown in Fig. 1. The upper and lower regions are half-spaces. The non-parallel interfaces are randomly deformed over an area $L \times L$. Two consecutive surfaces are separated by a layer with thickness $d_i = u_i - u_{i-1}$ (with $2 \leq i \leq N-1$).

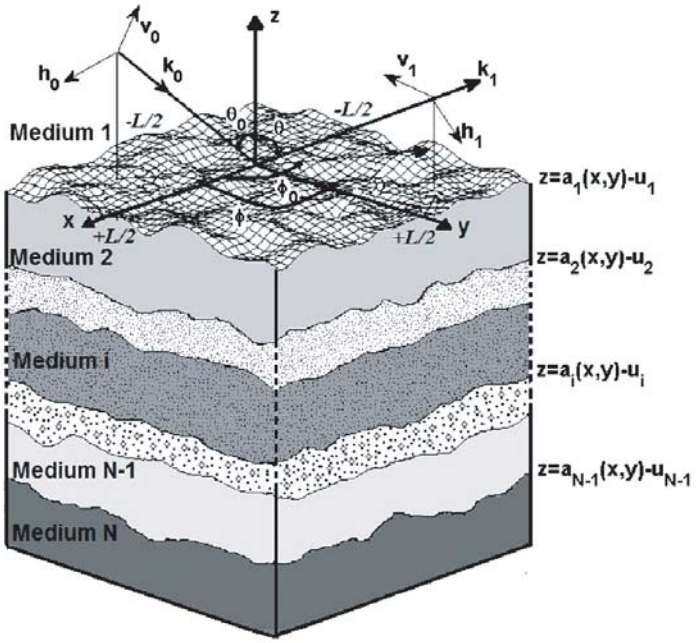

Figure 1. Structure with several two-dimensional rough interfaces.

The functions $a_i(x, y)$ are realizations of second order stationary and centered Gaussian random processes. They can be obtained from the filtering of white Gaussian noise realizations $b_j(x, y)$ [4]:

$$a_i(x,y) = h_i(x,y) * \sum_{j=1}^{N-1} p_{ij} b_j(x,y) \tag{1}$$

The star symbol $(*)$ designates the convolution operation in the spatial domain. The function $h_i(x, y)$ is the impulse response of the filter associated with the interface i and the coefficients p_{ij} are the primary mixing parameters. Knowing that the white noises are uncorrelated, the statistical correlation $R_{ij}(x, y)$ between the interfaces i and j (with $1 \leq (i; j) \leq N-1$) is given by:

$$R_{ij}(x,y) = \langle a_i(x',y') a_j(x+x', y+y') \rangle = q_{ij} C_{ij}(x,y) \tag{2}$$

The angular brackets stand for statistical averages. The coefficients q_{ij} are the secondary mixing parameters defined by $q_{ij} = \sum_{k=1}^{N-1} p_{ik}p_{jk}$ with $|q_{ij}| \leq 1$ and $q_{ii} = 1$. The function $C_{ij}(x, y)$ is the correlation function between $h_i(x, y)$ and $h_j(x, y)$.

The spectrum $\hat{R}_{ii}(\alpha, \beta)$ and the cross-spectrum $\hat{R}_{i,j\neq i}(\alpha, \beta)$ are the Fourier transforms of auto- and cross-correlations $R_{ii}(x, y)$ and $R_{i,j\neq i}(x, y)$ with:

$$\hat{R}_{ij}(\alpha, \beta) = q_{ij}\hat{h}_i^*(\alpha, \beta)\hat{h}_j(\alpha, \beta) \tag{3}$$

The function $\hat{h}_i(\alpha, \beta)$ is the transfer function of the filter associated with the interface i. The superscript asterisk indicates the conjugate complex. For the numerical applications, we consider the statistical autocorrelations $R_{ii}(x, y)$ under the following form:

$$R_{ii}(x, y) = \sigma_i^2 \exp\left[-\left(\sqrt{\frac{x^2}{l_{xi}^2} + \frac{y^2}{l_{yi}^2}}\right)^{2H}\right] \tag{4}$$

The interface i is characterized by the root-mean-square height σ_i and the correlation lengths l_{xi} and l_{yi}. The interface is isotropic if $l_{xi} = l_{yi}$ and anisotropic if $l_{xi} \neq l_{yi}$. The autocorrelation function $R_{ii}(x, y)$ is Gaussian when the roughness exponent H is equal to 1 and it is a bi-exponential function when $H = 0.5$. The spectrum $\hat{R}_{ii}(\alpha, \beta)$ is expressed in the following form:

$$\hat{R}_{ii}(\alpha, \beta) = \sigma_i^2 l_{xi} l_{yi} \pi \exp\left(-\frac{\alpha^2 l_{xi}^2 + \beta^2 l_{yi}^2}{4}\right) \quad \text{if } H = 1 \tag{5}$$

$$\hat{R}_{ii}(\alpha, \beta) = \frac{2\pi\sigma_i^2 l_{xi} l_{yi}}{\left(1 + \alpha^2 l_{xi}^2 + \beta^2 l_{yi}^2\right)^{3/2}} \quad \text{if } H = 0.5 \tag{6}$$

We determine the filter transfer functions $h_i(x, y)$ from the relations in Eqs. (3) and (5) or Eq. (6). The solution is not unique, and we suppose real-valued transfer functions. In this case, the cross-spectrum is given in the following forms:

$$\hat{R}_{ij}(\alpha, \beta) = q_{ij}\sigma_i\sigma_j\pi\sqrt{l_{xi}l_{xj}l_{yi}l_{yj}} \exp\left[-\alpha^2\frac{\left(l_{xi}^2 + l_{xj}^2\right)}{8} - \beta^2\frac{\left(l_{yi}^2 + l_{yj}^2\right)}{8}\right] \quad \text{if } H = 1 \tag{7}$$

$$\hat{R}_{ij}(\alpha, \beta) = q_{ij}\frac{2\pi\sigma_i\sigma_j\sqrt{l_{xi}l_{xj}l_{yi}l_{yj}}}{\left(1 + \alpha^2 l_{xi}^2 + \beta^2 l_{yi}^2\right)^{3/4}\left(1 + \alpha^2 l_{xj}^2 + \beta^2 l_{yj}^2\right)^{3/4}} \quad \text{if } H = 0.5 \tag{8}$$

3. SCATTERED INTENSITY

The structure is illuminated by a horizontal (h) or vertical (v) polarized plane wave with a wavelength λ. The time dependence is assumed to be in $\exp(j\omega t)$. The top region is assimilated to the vacuum. Each layer is characterized by a relative permittivity ε_{r_i} and a wave number $k_i = \sqrt{\varepsilon_{r_i}}k_0$ where k_0 is the vacuum wave number. The incident wave vector $\mathbf{k}_0(\alpha_0, \beta_0, -\gamma_0)$ is defined by the zenith angle θ_0 and the azimuth angle ϕ_0 (Fig. 1) with $\alpha_0 = k_1 \sin\theta_0 \cos\phi_0$, $\beta = k_1 \sin\theta_0 \sin\phi_0$ and $\gamma_0 = k_1 \sin\theta_0$.

The small perturbation method gives the first-order scattering amplitude $A_{(ba)}^{(1)}(\theta, \phi)$ of the field scattered within the vacuum as follows [3–6]:

$$A_{(ba)}^{(1)}(\theta, \phi) = \sum_{i=1}^{N-1} K_{i,(ba)}(\alpha, \beta)\hat{a}_i(\alpha - \alpha_0, \beta - \beta_0) \tag{9}$$

The subscript (a) denotes the incident wave polarization (h or v) and the subscript (b), the scattered wave polarization (h or v). The propagation coefficients α and β of the scattered wave are defined from

the zenith angle θ and the azimuth angle ϕ with $\alpha = k_1 \sin\theta\cos\phi$ and $\beta = k_1 \sin\theta\sin\phi$. The function $\hat{a}_i(\alpha,\beta)$ is the Fourier transform of the function $a_i(x,y)$. The first-order SPM kernels $K_{i,(ba)}(\alpha,\beta)$ can be obtained by an iterative formula as shown in [6] and they depend on the layer thickness values and the relative permittivity values and on the incidence and scattering angles. We established in [1] the analytical expressions of the first-order SPM kernels $k_{1,(ba)}(\alpha,\beta)$ and $k_{2,(ba)}(\alpha,\beta)$ for a stratified structure with two rough interfaces. In appendix, we give the analytical expressions in the case of three interfaces. To our knowledge, it is the first time that these closed-form formulas are presented.

The normalized scattering intensity $I_{(ba)}(\theta,\phi)$ represents the power scattered in the direction (θ, ϕ) per unit of solid angle divided by the incident power,

$$I_{(ba)}(\theta,\phi) = \frac{\cos^2\theta}{\lambda^2\cos\theta_0 L^2}\left|A^{(1)}_{(ba)}(\theta,\phi)\right|^2 \tag{10}$$

where $-\pi/2 \le \theta \le +\pi/2$ and $0 \le \phi \le \pi$. For a layered structure with randomly rough boundaries, the normalized scattering intensity $I_{(ba)}(\theta,\phi)$ depends on rough boundary height profile realizations and for a given direction, it is a random variable.

Within the framework of the first-order SPM and when $L \to +\infty$, the average scattering intensity $\langle I_{(ba)}\rangle$ is given by:

$$\langle I_{(ba)}(\theta,\phi)\rangle = \frac{\cos^2\theta}{\lambda^2\cos\theta_0}\sum_{i=1}^{N-1}\sum_{j=1}^{N-1}\mathrm{Re}\left[K_{i(ba)}(\alpha,\beta)K^*_{j(ba)}(\alpha,\beta)\hat{R}_{ij}(\alpha-\alpha_0,\beta-\beta_0)\right] \tag{11}$$

4. STATISTICAL DISTRIBUTION OF THE LRSI

Let $V_{(ba,b'a')} = I_{ba}/I_{b'a'}$ the intensity ratio associated with the components (ba) and $(b'a')$ of the wave scattered in the direction (θ, ϕ). For infinite surface areas ($L \to +\infty$) and centered Gaussian height distributions, we demonstrated in [8] that the PDF $p_{V_{(ba,b'a')}}(v)$ of $V_{(ba,b'a')}$ is given by:

$$p_{V_{(ba,b'a')}}(v) = (1-r^2)p_0\frac{v+p_0}{[(v+p_0)^2 - 4vp_0r^2]^{3/2}} \tag{12}$$

The PDF $p_{V_{(ba,b'a')}}(v)$ is fully determined by the knowledge of the two parameters p_0 and r.

$$p_0 = \frac{\langle I_{ba}\rangle}{\langle I_{b'a'}\rangle} \tag{13}$$

and,

$$r = \sqrt{\frac{\Gamma^2_{R_{ba}R_{b'a'}} + \Gamma^2_{R_{ba}I_{b'a'}}}{\sigma^2_{R_{ba}}\sigma^2_{R_{b'a'}}}} \tag{14}$$

The quantity r designates the correlation coefficient of the two complex random variables $A^{(1)}_{(ba)}(\theta,\phi)$ and $A^{(1)}_{(b'a')}(\theta,\phi)$ [1, 8] and its value lies between 0 and 1. The quantity $\sigma^2_{R_{ba}}$ is the variance of the real part of the scattering amplitude $A^{(1)}_{(ba)}(\theta,\phi)$. The quantity $\Gamma_{R_{ba}R_{b'a'}}$ (and $\Gamma_{R_{ba}I_{b'a'}}$) is the covariance between the real parts of $A^{(1)}_{(ba)}(\theta,\phi)$ and $A^{(1)}_{(b'a')}(\theta,\phi)$ (and, between the real and imaginary parts, respectively). These statistical moments are defined by [9]:

$$\sigma^2_{R_{ba}} = \frac{1}{2}\sum_{i=1}^{N-1}\sum_{j=1}^{N-1}\mathrm{Re}\left[K_{i,(ba)}K^*_{j,(ba)}\hat{R}_{ij}(\alpha-\alpha_0,\beta-\beta_0)\right] \tag{15}$$

$$\Gamma_{R_{ba}R_{b'a'}}(\alpha,\beta) = \frac{1}{2}\sum_{i=1}^{N-1}\sum_{j=1}^{N-1}\mathrm{Re}\left[K^*_{i,(ba)}K_{j,(b'a')}\hat{R}_{ij}(\alpha-\alpha_0,\beta-\beta_0)\right] \tag{16}$$

$$\Gamma_{R_{ba}I_{b'a'}}(\alpha,\beta) = \frac{1}{2}\sum_{i=1}^{N-1}\sum_{j=1}^{N-1}\mathrm{Im}\left[K^*_{i,(ba)}K_{j,(b'a')}\hat{R}_{ij}(\alpha-\alpha_0,\beta-\beta_0)\right] \tag{17}$$

Let $S_{(b'a',ba)} = I_{b'a'}/(I_{ba} + I_{b'a'})$ be the LRSI associated with the components $(b'a')$ and (ba) of the scattered wave in the direction $(\theta,\, \phi)$. The random variable $S_{(b'a',ba)}$ takes values in $[0, +1]$. Knowing that $S_{(b'a',ba)} = 1/(V_{(ba,b'a')} + 1)$, we determine the PDF of $S_{(b'a',ba)}$ from the following transformation:

$$p_{S_{(b'a',ba)}}(s) = \left|\frac{dv(s)}{ds}\right| p_{V_{(ba,b'a')}}(v(s)) = \frac{1}{s^2} p_{V_{(ba,b'a')}}(v(s)) \tag{18}$$

where $s = 1/(v+1)$ and $v = I_{ba}/I_{b'a'}$, and we find:

$$p_S(s) = \frac{p_0\left(1-r^2\right)\left[s(p_0-1)+1\right]}{\left\{s^2\left[(p_0-1)^2+4p_0r^2\right]+2s\left[(p_0-1)-2p_0r^2\right]+1\right\}^{3/2}} \tag{19}$$

We show that when $p_0 > 1$ and $r^2 \in \left]0, \frac{p_0-1}{3p_0}\right]$ or when $0 < p_0 < 1$ and $r^2 \in \left]\frac{1-p_0}{3}, 1\right]$, the PDF is maximum for $s = s_0$ with:

$$s_0 = \frac{\left[2(1-p_0)^2 + r^2p_0(7-p_0)\right] - rp_0\sqrt{r^2\left(p_0^2+34p_0+1\right)+8(1-p_0)^2}}{2(1-p_0)\left[(1-p_0)^2+4r^2p_0\right]} \tag{20}$$

When $p_0 > 1$ and $r^2 \in \left]0, \frac{p_0-1}{3p_0}\right]$, the PDF is a decreasing function over $[0; 1]$ and $s_0 = 0$. When $0 < p_0 < 1$ and $r^2 \in \left]0, \frac{1-p_0}{3}\right]$, the PDF increases over $[0; 1]$ and $s_0 = 1$.

The CDF of the continuous random variable $S_{(b'a',ba)}$ can be expressed as the integral of its PDF in Eq. (19), and we find:

$$F_S(s) = \frac{1}{2} + \frac{s(p_0+1)-1}{2\left\{s^2\left[(p_0-1)^2+4p_0r^2\right]+2s\left[(p_0-1)-2p_0r^2\right]+1\right\}^{1/2}} \tag{21}$$

We deduce from Eq. (21) that the median M_n of $S_{(b'a',ba)}$ is equal to $1/(1+p_0)$. Knowing that $\langle I_{(ba)}\rangle = p_0\langle I_{(b'a')}\rangle$, the median is equal to $\frac{\langle I_{(b'a')}\rangle}{\langle I_{(ba)}\rangle+\langle I_{(b'a')}\rangle}$.

As shown by the relations in Eqs. (13) to (17), through the first-order SPM Kernels $K_{i,(ba)}(\alpha,\beta)$ and the co- and cross-spectra $\hat{R}_{ij}(\alpha,\beta)$, the two parameters p_0 and r depend on the layer thickness values and the relative permittivity values, on the incidence and scattering angles and on the statistical parameters of all rough boundaries. For a structure with one, two or three slightly rough surfaces, the analytical expressions for both parameters p_0 and r can be derived from the co- and cross-spectrum formulas (Eqs. (5) to (8)) and from the closed-form formulas given in the appendix for the SPM-Kernels.

For a given observation direction, the random variable $V_{(ba,b'a')}$ follows a heavy-tailed distribution and does not have a finite mean and a finite variance [8]. In contrast, the mean and the variance of $S_{(b'a',ba)}$ are finite. After some mathematical operations, we find the first- and second-order moments as follows:

$$\begin{aligned}\langle S_{(b'a',ba)}\rangle \;=\; & \frac{2p_0r^2-(p_0-1)}{(p_0-1)^2+4p_0r^2} \\ & + \frac{p_0(p_0-1)(1-r^2)}{\left[(p_0-1)^2+4p_0r^2\right]^{3/2}} \ln\left(p_0\frac{\sqrt{(p_0-1)^2+4p_0r^2}+(p_0-1)+2r^2}{\sqrt{(p_0-1)^2+4p_0r^2}+(p_0-1)-2p_0r^2}\right)\end{aligned} \tag{22}$$

$$\begin{aligned}\langle S^2_{(b'a',ba)}\rangle \;=\; & \frac{(p_0+1)\left[(p_0-1)^2+p_0r^2(3-p_0)\right]-8p_0^2r^2(1-r^2)}{\left[(p_0-1)^2+4p_0r^2\right]^2} \\ & + \frac{2p_0(1-r^2)\left[p_0r^2(3p_0-1)-(p_0-1)^2\right]}{\left[(p_0-1)^2+4p_0r^2\right]^{5/2}} \ln\left[p_0\frac{\sqrt{(p_0-1)^2+4p_0r^2}+(p_0-1)+2r^2}{\sqrt{(p_0-1)^2+4p_0r^2}+(p_0-1)-2p_0r^2}\right]\end{aligned} \tag{23}$$

We deduce from Eqs. (22) and (23) the variance with $\sigma^2_{S_{(b'a',ba)}} = \langle S^2_{(b'a',ba)}\rangle - \langle S_{(b'a',ba)}\rangle^2$.

When $r = 1$, the LRSI remains unchanged from a stratified structure realization to another, and we have Prob $\left\{S_{(b'a',ba)} = 1/(1+p_0)\right\} = 1$. When $r = 0$ and $p_0 = 1$, the PDF does not contain information about the stratified medium because the random variable $S_{(b'a',ba)}$ is uniformly distributed between 0 and 1. In this case, we have: $\langle S_{(b'a',ba)}\rangle = 1/2$ and $\langle S^2_{(b'a',ba)}\rangle = 1/3$.

5. NUMERICAL RESULTS

We consider a stratified medium air/clayey soil/rock with or without a snow layer. A h- or v-polarized plane wave of wavelength $\lambda = 30\,\text{cm}$ impinges on the structure under the angles $\theta_0 = 30°$ and $\phi_0 = 0°$. We consider Gaussian and exponential function correlations with the rms-heights $\sigma_1 = 0.015\lambda$, $\sigma_2 = 0.022\lambda$ and $\sigma_3 = 0.023\lambda$ and the correlation lengths $l_{x1} = l_{y1} = 0.2\lambda$ or $l_{y1} = 2l_{x1} = 0.4\lambda$, $l_{x2} = l_{y2} = 0.25\lambda$ and $l_{x3} = l_{y3} = 0.3\lambda$. The average thickness of the snow layer under consideration is $d_2 = 0.35\lambda$ and that of the clayey layer is $d_3 = 2\lambda$. The relative permittivity values are $\varepsilon_{r1} = 1$, $\varepsilon_{r2} = 3$, $\varepsilon_{r3} = 9.5 - i0.00055$ and $\varepsilon_{r4} = 20.5 - i2.55$ [4]. The first configuration (C1) under study has no snow cover, and the other three configurations (C2, C3 and C4) have one. For configuration C1, the air/clayey soil and clayey soil/rock boundaries are isotropic and uncorrelated. For configuration C2, all interfaces are isotropic and uncorrelated. For configuration C3, the air/snow boundary is anisotropic with $l_{y1} = 2l_{x1} = 0.4\lambda$, but all interfaces are uncorrelated. For configuration C4, all interfaces are isotropic. The snow/clayey soil and clayey soil/rock boundaries and the air/snow and clayey-soil/rock boundaries are not correlated with $q_{23} = q_{13} = 0$. By contrast, the air/snow and snow/clayey soil interfaces are highly correlated with $q_{12} = 9/10$. We have analyzed these configurations in [1] by using the probability law of the co- and cross-polarized intensity ratios $V_{(bb,aa)}$ and $V_{(ba,aa)}$. Here we analyze these 4 configurations by using the statistical distribution of the LRSI for which the mean and standard deviation are defined. Moreover, we consider boundaries with Gaussian and non-Gaussian spectra.

Figure 2 shows the theoretical PDFs of $S_{(vv,hh)} = I_{vv}/(I_{hh} + I_{vv})$ in the backscattering direction $\theta = -30°$ for the four configurations. The theoretical PDFs are given by Eq. (19). For the four configurations and the two types of correlation functions, the Table 1 gives the two parameters r and p_0 obtained from Eqs. (13) and (14), the mean $\langle S_{(vv,hh)} \rangle$, obtained from Eq. (22), the standard deviation $\sigma_{S_{(vv,hh)}}$ derived from Eqs. (22) and (23) and the maximum position s_0 obtained from Eq. (20). The PDF-curves change weakly from one correlation function to another because the two parameters p_0 and r defining the probability law depend very little on the correlation function. For example, for the configuration C1, we find $p_0 = 0.576$ and $r = 0.991$ in the Gaussian case and $p_0 = 0.568$ and $r = 0.991$ in the non-Gaussian case, respectively. In fact, the determining factor upon the properties of the LRSI is the snow cover. The largest value of the standard deviation $\sigma_{S_{(vv,hh)}}$ is found for configuration (C1) without the snow layer. Consequently, for the three structures with the snow layer, the PDF curve is narrower and the maximum value is therefore higher. The cross-correlation (C4) compared with

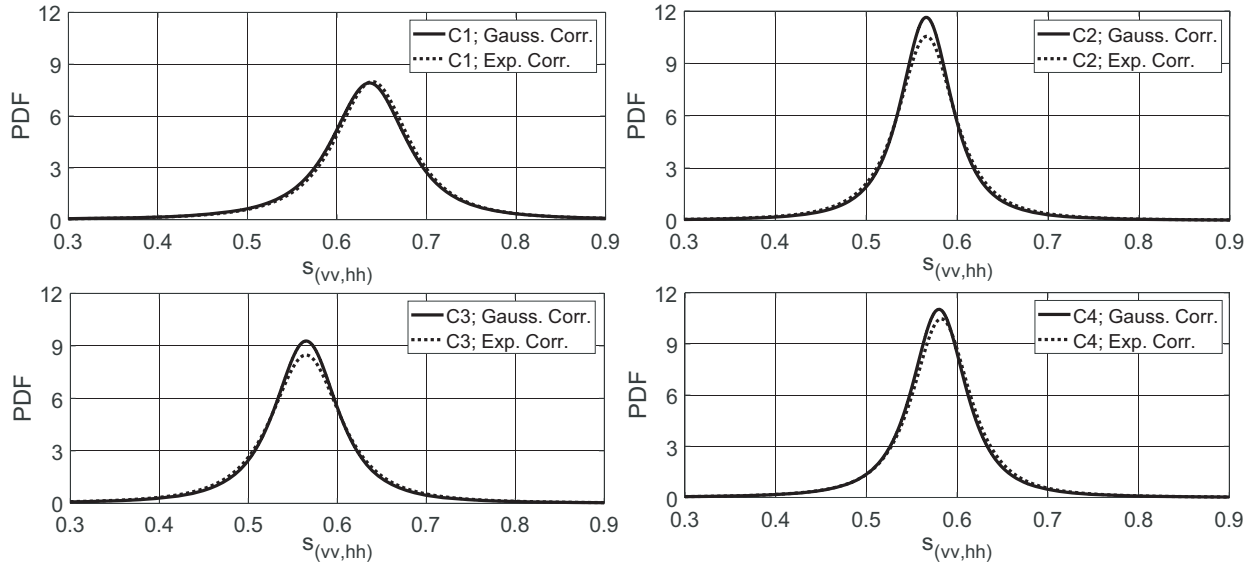

Figure 2. PDF of $S_{(vv,hh)}$ in the backscattering direction for the 4 configurations with Gaussian and exponential correlation functions.

Table 1. Values of r, p_0, $\langle S \rangle$, σ_S and s_0 characterizing the random variable $S_{(vv,hh)}$ in the backscattering direction for the four configurations.

	Correlation	C1	C2	C3	C4
r	Gauss.	0.991	0.996	0.994	0.996
	Exp.	0.991	0.995	0.993	0.995
p_0	Gauss.	0.576	0.768	0.772	0.726
	Exp.	0.568	0.767	0.773	0.718
$\langle S \rangle$	Gauss.	0.631	0.565	0.563	0.578
	Exp.	0.634	0.565	0.563	0.580
σ_S	Gauss.	0.0858	0.0634	0.0755	0.0662
	Exp.	0.0852	0.0685	0.0809	0.0689
s_0	Gauss.	0.636	0.566	0.565	0.580
	Exp.	0.640	0.566	0.565	0.583

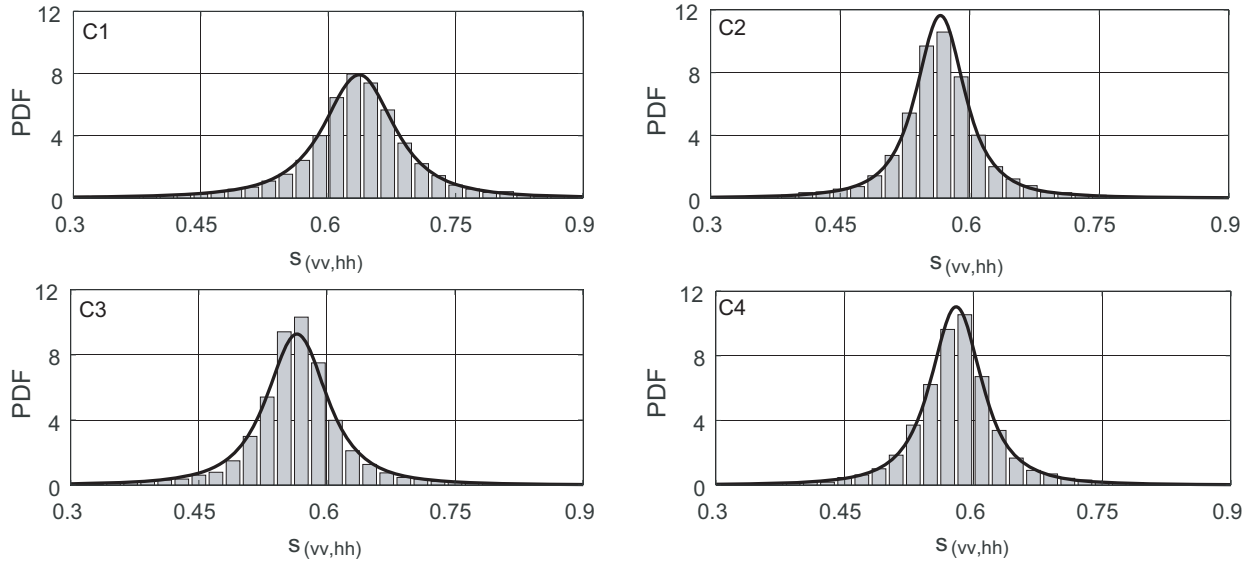

Figure 3. Theoretical PDF of $S_{(vv,hh)}$ and normalized histogram in the backscattering direction for the 4 configurations with Gaussian correlation functions.

configuration (C2) where the three interfaces are isotropic and uncorrelated causes a little shift in the peak position and the anisotropy (C3), a slight decrease in the maximum value. We can also note that the snow layer causes an increase in the value of s_0 and as a result, a shift of the maximum to the left. If we consider the random variable $S_{(hh,vv)}$ in place of $S_{(vv,hh)}$, the shift occurs on the right.

Figure 3 shows the PDFs of $S_{(vv,hh)}$ in a backscattering $\theta = -30°$ and the normalized histograms derived from Monte-Carlo simulations for Gaussian correlation functions. The histograms are derived from 5000 results obtained with the relations in Eqs. (9) and (10) and estimated on areas of $900\lambda^2$. Comparisons are good and confirm the validity of the analytical formulation in the backscattering direction.

Figure 4 shows the PDF of the cross-polarized $S_{(hv,vv)} = I_{hv}/(I_{hv} + I_{vv})$ under the observation direction defined by $\theta = -50°$ and $\phi = 40°$. Table 2 gives the parameter values of the random variable $S_{(hv,vv)}$. We can draw similar conclusions to the previous case. The key factor influencing the probability law of the LRSI is the snow cover. The PDF weakly changes from one correlation function to another

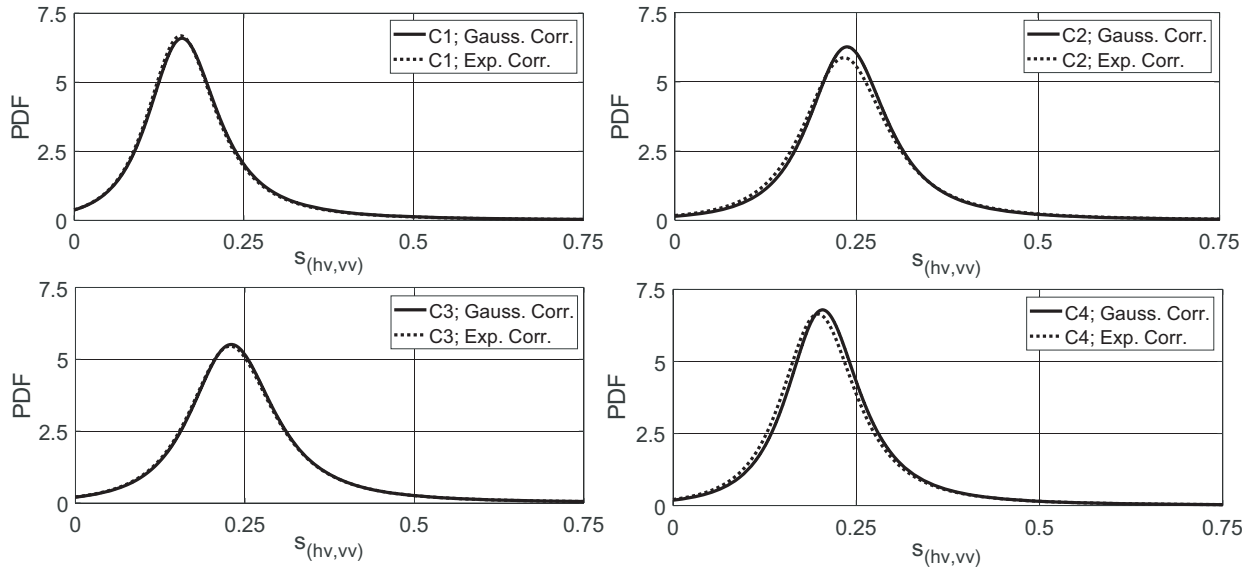

Figure 4. PDF of $S_{(hv,vv)}$ under the observation direction defined by $\theta = -50°$ and $\phi = 40°$ for the 4 configurations with Gaussian and exponential correlation functions.

Table 2. Values of r, p_0, $\langle S \rangle$, σ_S and s_0 characterizing the random variable $S_{(hv,vv)}$ in the observation direction ($\theta = -50°$; $\phi = 40°$) for the four configurations.

	Correlation	C1	C2	C3	C4
r	Gauss.	0.961	0.976	0.968	0.975
	Exp.	0.961	0.972	0.967	0.972
p_0	Gauss.	4.92	3.11	3.20	3.75
	Exp.	5.00	3.17	3.22	3.88
$\langle S \rangle$	Gauss.	0.188	0.256	0.255	0.225
	Exp.	0.186	0.254	0.254	0.220
σ_S	Gauss.	0.109	0.106	0.117	0.102
	Exp.	0.108	0.112	0.118	0.104
s_0	Gauss.	0.159	0.237	0.230	0.204
	Exp.	0.157	0.233	0.228	0.198

and we can note that for this observation direction, the standard deviation weakly changes from one configuration to another. But the lowest value of the mean $\langle S_{(hv,vv)} \rangle$ is found for configuration (C1) without the snow layer. When there is a snow layer, the maximum of the PDF of $S_{(hv,vv)}$ is shifted to the right.

Figure 5 gives the $S_{(hv,vv)}$ PDF curves and the normalized histograms obtained from Monte-Carlo simulations for the observation direction defined by $\theta = -50°$ and $\phi = 40°$ and for the non-Gaussian spectra. As in the backscattering direction, the comparisons are conclusive and validate the closed-formulae for the PDF of the cross-polarized LRSI in the case of non-Gaussian correlation functions.

Figure 6 shows the PDF curves of the random variable $S_{(hv,vv)}$ under the observation direction defined by $\theta = 60°$ and $\phi = 90°$. Table 3 gives the values of parameters associated with $S_{(hv,vv)}$. As shown previously, the PDF weakly changes from one correlation function to another. In contrast, the influence of snow cover upon the probability law of the LRSI is well marked. The largest value of the standard deviation $\sigma_{S_{(vv,hh)}}$ is found for configuration (C1) without the snow layer. For the three

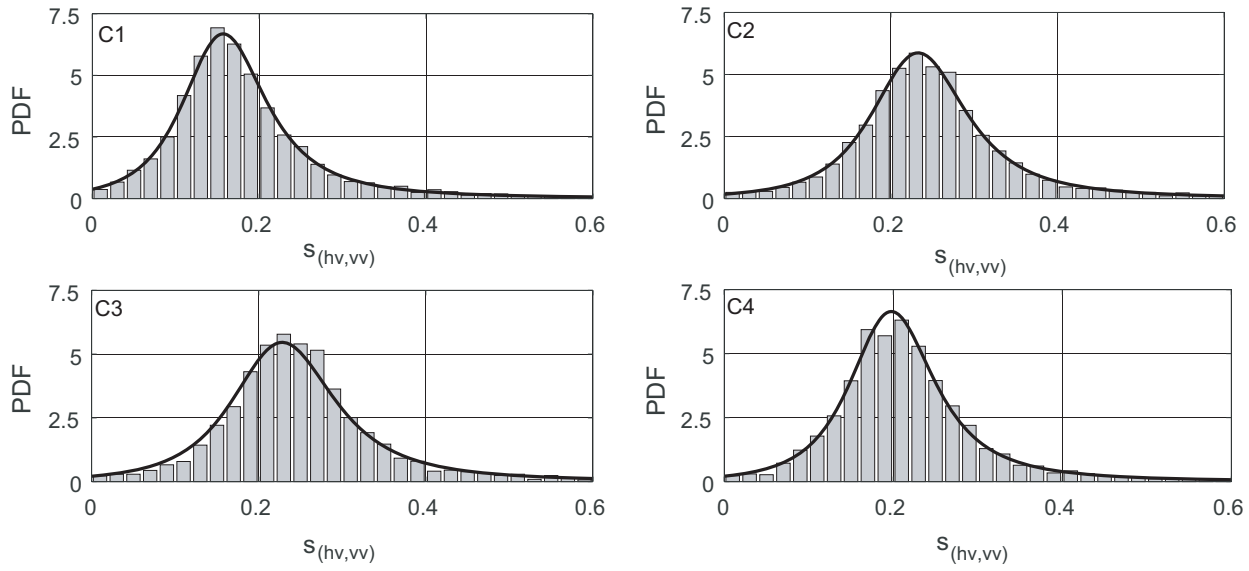

Figure 5. Theoretical PDF of $S_{(hv,vv)}$ and normalized histogram for the 4 configurations with exponential correlation functions under $\theta = -50°$ and $\phi = 40°$.

Table 3. Values of r, p_0, $\langle S \rangle$, σ_S and s_0 characterizing the random variable $S_{(hv,vv)}$ in the observation direction ($\theta = 60°$; $\phi = 90°$) for the four configurations.

	Correlation	C1	C2	C3	C4
r	Gauss.	0.723	0.547	0.565	0.701
	Exp.	0.744	0.537	0.589	0.717
p_0	Gauss.	0.393	0.102	0.0903	0.167
	Exp.	0.423	0.129	0.0880	0.204
$\langle S \rangle$	Gauss.	0.670	0.839	0.852	0.795
	Exp.	0.659	0.814	0.856	0.770
σ_S	Gauss.	0.228	0.187	0.178	0.195
	Exp.	0.227	0.200	0.174	0.202
s_0	Gauss.	0.810	1	0.997	0.940
	Exp.	0.784	1	0.993	0.917

configurations with the snow cover, the PDF curves are narrower and the standard derivation value are therefore smaller. For configurations C2, $0 < p_0 < 1$ and $r^2 \in \left]0, \frac{1-p_0}{3}\right]$. Consequently, the PDF is an increasing function and attains its maximum when $s = s_0 = 1$. We can always observe that when there is a snow layer, the maximum of the PDF of $S_{(hv,vv)}$ is shifted to the right.

Figure 7 shows the PDF of the random variable $S_{(hv,vv)}$ associated with the observation direction $\theta = 60°$ and $\phi = 90°$ in the Gaussian case and the normalized histograms obtained from 5000 Monte-Carlo simulations. As for both previous observation directions, the comparisons are conclusive and validate the analytical expressions for the probability law of the LRSI obtained within the framework of the first-order SPM.

The two parameters p_0 and r are defined from the first-order SPM kernels and the co- and cross-spectra of rough interfaces. Consequently, the values of both parameters change with the snow cover thickness, but for the configurations under study, the LRSI-PDF allows to differentiate the cases with and without the snow cover when the snow layer thickness is greater than $\lambda/10$.

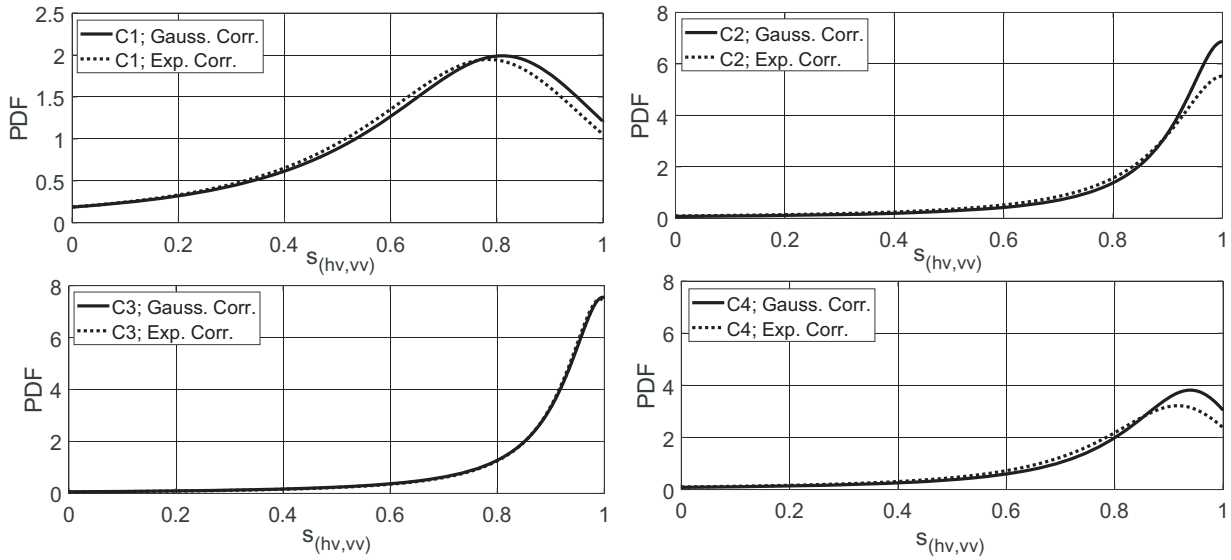

Figure 6. PDF of $S_{(hv,vv)}$ in the perpendicular plane for the 4 configurations with Gaussian and exponential correlation functions.

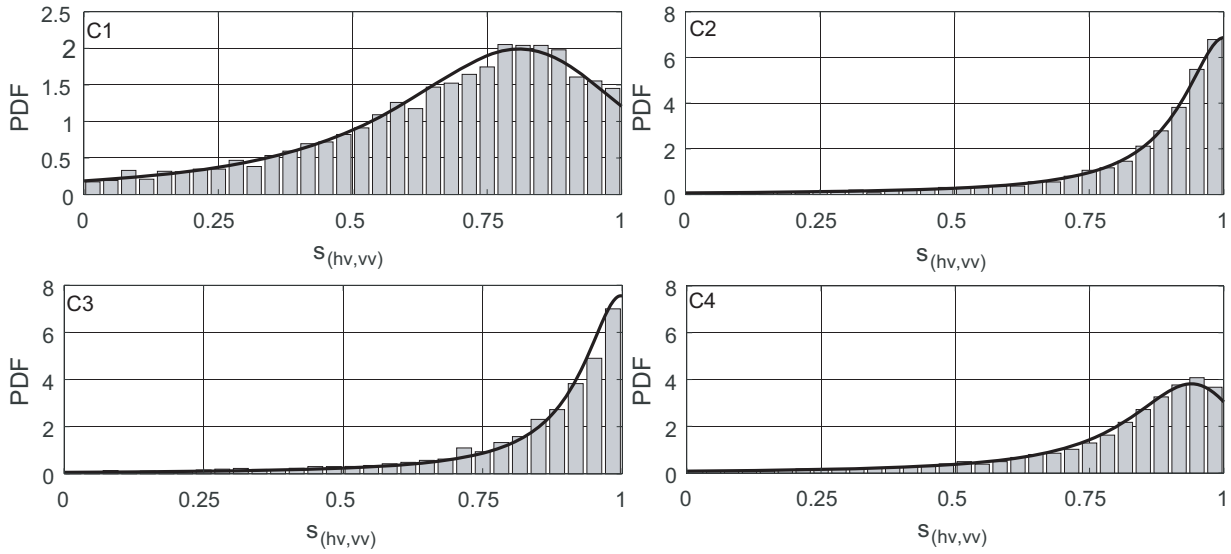

Figure 7. Theoretical PDF of $S_{(hv,vv)}$ and normalized histogram in the perpendicular plane for the 4 configurations with Gaussian correlation functions.

6. CONCLUSION

In this paper we look for the statistical properties of the co- and cross-polarized Layered Rough Surface Index (LRSI) for three-dimensional layered structures with an arbitrary number of slightly rough boundaries and illuminated by an electromagnetic plane wave. For infinite surface areas and Gaussian centered height distributions, we have shown within the framework of the first-order small perturbation method that the probability density function and the cumulative density function of the LRSI are fully determined by two parameters that depend on the layer thickness values and the relative permittivity values, on the incidence and scattering angles and on the statistical parameters of all rough boundaries. Contrary to the intensity ratio which follows a heavy-tailed distribution, the LRSI probability law has a finite mean and a finite variance whose analytic expressions we have established.

For a structure air/clayey soil/rock, we have analyzed the influence of a snow layer upon the probability laws in the cases of Gaussian and exponential correlation functions, and we have shown that the PDF shape is truly informative and allows to differentiate the cases with and without the snow cover. For the structure under study, the properties of the LRSI change weakly from one correlation function to another, and the determining factor upon the properties is the snow cover.

We have also compared the theoretical PDF curves and the normalized histograms derived from Monte-Carlo simulations. The comparisons are conclusive and validate the analytical expressions established in this paper. The LRSI statistics are useful tools for studying, characterizing and monitoring a land snow cover.

APPENDIX A. ANALYTICAL EXPRESSIONS OF THE FIRST-ORDER SPM KERNELS FOR A STRATIFIED STRUCTURE WITH THREE ROUGH INTERFACES

The first-order SPM kernels $K_{i,(ba)}$ can be obtained by an iterative formula as shown in [6]. We have derived from this formula the analytical expressions of $K_{i,(ba)}$ for a stack of three rough interfaces. We denote the mean thicknesses of the second and third layers by d_2 and d_3. For a h-polarized incident wave, the factors $K_{i,(hh)}(\alpha,\beta)$ and $K_{i,(vh)}(\alpha,\beta)$ associated with the progressive plane waves (i.e., for $\alpha = k_1 \sin\theta\cos\varphi$ and $\beta = k_1 \sin\theta\sin\varphi$) are defined as follows:

$$K_{1,(hh)} = j(k_1^2 - k_2^2)\frac{\gamma_{10}\cos(\varphi-\varphi_0)}{r_h(\gamma_0)r_h(\gamma)} \left\{ \begin{array}{l} \gamma_{30}\left[\gamma_{20}\cos(\gamma_{20}d_2)\cos(\gamma_{30}d_3) - \gamma_{30}\sin(\gamma_{20}d_2)\sin(\gamma_{30}d_3)\right] \\ +j\gamma_{40}\left[\gamma_{30}\sin(\gamma_{20}d_2)\cos(\gamma_{30}d_3) + \gamma_{20}\cos(\gamma_{20}d_2)\sin(\gamma_{30}d_3)\right] \end{array} \right\}$$
$$\times \left\{ \begin{array}{l} \gamma_3\left[\gamma_2\cos(\gamma_2 d_2)\cos(\gamma_3 d_3) - \gamma_3\sin(\gamma_2 d_2)\sin(\gamma_3 d_3)\right] \\ +j\gamma_4\left[\gamma_3\sin(\gamma_2 d_2)\cos(\gamma_3 d_3) + \gamma_2\cos(\gamma_2 d_2)\sin(\gamma_3 d_3)\right] \end{array} \right\} \quad \text{(A1)}$$

$$K_{2,(hh)} = j(k_2^2 - k_3^2)\frac{2\gamma_{10}\gamma_{20}\gamma_2\cos(\varphi-\varphi_0)}{r_{(h)}(\gamma)r_{(h)}(\gamma_0)}\left[\gamma_{30}\cos(\gamma_{30}d_3) + j\gamma_{40}\sin(\gamma_{30}d_3)\right]$$
$$\left[\gamma_3\cos(\gamma_3 d_3) + j\gamma_4\sin(\gamma_3 d_3)\right] \quad \text{(A2)}$$

$$K_{3,(hh)} = j(k_3^2 - k_4^2)\frac{2\gamma_{10}\gamma_{20}\gamma_{30}\gamma_2\gamma_3\cos(\varphi-\varphi_0)}{r_{(h)}(\gamma)r_{(h)}(\gamma_0)} \quad \text{(A3)}$$

$$K_{1,(vh)} = j(k_1^2 - k_2^2)\frac{2k_1\gamma_{10}\gamma_2\sin(\varphi-\varphi_0)}{r_{(v)}(\gamma)r_{(h)}(\gamma_0)} \left\{ \begin{array}{l} \gamma_{30}\left[\gamma_{20}\cos(\gamma_{20}d_2)\cos(\gamma_{30}d_3) - \gamma_{30}\sin(\gamma_{20}d_2)\sin(\gamma_{30}d_3)\right] \\ +j\gamma_{40}\left[\gamma_{30}\sin(\gamma_{20}d_2)\cos(\gamma_{30}d_3) + \gamma_{20}\cos(\gamma_{20}d_2)\sin(\gamma_{30}d_3)\right] \end{array} \right\}$$
$$\times \left\{ \begin{array}{l} k_3^2\gamma_4\left[k_2^2\gamma_3\cos(\gamma_2 d_2)\cos(\gamma_3 d_3) - k_3^2\gamma_2\sin(\gamma_2 d_2)\sin(\gamma_3 d_3)\right] \\ +jk_4^2\gamma_3\left[k_3^2\gamma_2\sin(\gamma_2 d_2)\cos(\gamma_3 d_3) + k_2^2\gamma_3\cos(\gamma_2 d_2)\sin(\gamma_3 d_3)\right] \end{array} \right\} \quad \text{(A4)}$$

$$K_{2,(vh)} = j(k_2^2 - k_3^2)\frac{2k_1k_2^2\gamma_{10}\gamma_{20}\gamma_2\gamma_3}{r_{(v)}(\gamma)r_{(h)}(\gamma_0)}\sin(\varphi-\varphi_0)\left[\gamma_{30}\cos(\gamma_{30}d_3) + j\gamma_{40}\sin(\gamma_{30}d_3)\right]$$
$$\times\left[k_3^2\gamma_4\cos(\gamma_3 d_3) + jk_4^2\gamma_3\sin(\gamma_3 d_3)\right] \quad \text{(A5)}$$

$$K_{3,(vh)} = j\frac{2\gamma_{10}\gamma_{20}\gamma_{30}\gamma_2\gamma_3\gamma_4 k_1 k_2^2 k_3^2 k_3^2 k_4^2}{r_h(\gamma_0)r_v(\gamma)}\sin(\varphi-\varphi_0) \quad \text{(A6)}$$

where

$$\begin{aligned} r_h(\gamma) \;=\; & \gamma_2\gamma_3(\gamma_1+\gamma_4)\cos(\gamma_2 d_2)\cos(\gamma_3 d_3) - \left(\gamma_2^2\gamma_4 + \gamma_1\gamma_3^2\right)\sin(\gamma_2 d_2)\sin(\gamma_3 d_3) \\ & +j\left[\gamma_2\left(\gamma_1\gamma_4 + \gamma_3^2\right)\cos(\gamma_2 d_2)\sin(\gamma_3 d_3) + \gamma_3\left(\gamma_2^2 + \gamma_1\gamma_4\right)\sin(\gamma_2 d_2)\cos(\gamma_3 d_3)\right] \end{aligned} \quad \text{(A7)}$$

and

$$\begin{aligned} r_v(\gamma) \;=\; & k_2^2k_3^2\gamma_2\gamma_3\left(\gamma_1k_4^2 + k_1^2\gamma_4\right)\cos(\gamma_2 d_2)\cos(\gamma_3 d_3) - \left(k_1^2k_3^4\gamma_2^2\gamma_4 + k_2^4k_4^2\gamma_1\gamma_3^2\right)\sin(\gamma_2 d_2)\sin(\gamma_3 d_3) \\ & +j\Big[k_3^2\gamma_3\left(k_1^2k_4^2\gamma_2^2 + k_2^4\gamma_1\gamma_4\right)\sin(\gamma_2 d_2)\cos(\gamma_3 d_3) \\ & +k_2^2\gamma_2\left(k_1^2k_4^2\gamma_3^2 + k_3^4\gamma_1\gamma_4\right)\cos(\gamma_2 d_2)\sin(\gamma_3 d_3)\Big] \end{aligned} \quad \text{(A8)}$$

The quantities r_{0h} and r_{0v} are deduced from Eqs. (A7) and (A8) with $r_{0h} = r_h(\alpha_0, \beta_0)$ and $r_{0v} = r_v(\alpha_0, \beta_0)$. The propagation coefficients γ_i and γ_{i0} are defined as $\gamma_i(\alpha, \beta) = \sqrt{k_i^2 - \alpha^2 - \beta^2}$ and $\gamma_{i0} = \gamma_i(\alpha_0, \beta_0)$.

For a v-polarized incident wave, the co- and cross-polarized SPM-kernels $K_{i,vv}(\alpha, \beta)$ and $K_{i,hv}(\alpha, \beta)$ are given as follows:

$$K_{1,(vv)} = \frac{j2\gamma_{10}(k_1^2 - k_2^2)}{r_v(\gamma_0) r_v(\gamma)} \times \left\{ \begin{array}{l} k_2^2 \chi\chi_0 \left[\begin{array}{l} k_4^2\gamma_3 \left(k_3^2\gamma_2 \cos(\gamma_2 d_2)\cos(\gamma_3 d_3) - k_2^2\gamma_3 \sin(\gamma_2 d_2)\sin(\gamma_3 d_3)\right)\big) \\ +jk_3^2\gamma_4 \left(k_3^2\gamma_2 \cos(\gamma_2 d_2)\sin(\gamma_3 d_3) + k_2^2\gamma_3 \sin(\gamma_2 d_2)\cos(\gamma_3 d_3)\right) \end{array} \right] \\ \times \left[\begin{array}{l} k_4^2\gamma_{30} \left(k_3^2\gamma_{20} \cos(\gamma_{20} d_2)\cos(\gamma_{30} d_3) - k_2^2\gamma_{30} \sin(\gamma_{20} d_2)\sin(\gamma_{30} d_3)\right) \\ +jk_3^2\gamma_{40} \left(k_2^2\gamma_{30} \sin(\gamma_{20} d_2)\cos(\gamma_{30} d_3) + k_3^2\gamma_{20} \cos(\gamma_{20} d_2)\sin(\gamma_{30} d_3)\right) \end{array} \right] \\ -k_1^2\gamma_2\gamma_{20}\cos(\varphi - \varphi_0) \left[\begin{array}{l} k_3^2\gamma_4 \big(k_2^2\gamma_3 \cos(\gamma_2 d_2)\cos(\gamma_3 d_3) - k_3^2\gamma_2 \sin(\gamma_2 d_2)\sin(\gamma_3 d_3)\big) \\ +jk_4^2\gamma_3 \big(k_3^2\gamma_2 \sin(\gamma_2 d_2)\cos(\gamma_3 d_3) + k_2^2\gamma_3 \cos(\gamma_2 d_2)\sin(\gamma_3 d_3)\big) \end{array} \right] \\ \times \left[\begin{array}{l} k_3^2\gamma_{40} \left(k_2^2\gamma_{30} \cos(\gamma_{20} d_2)\cos(\gamma_{30} d_3) - k_3^2\gamma_{20} \sin(\gamma_{20} d_2)\sin(\gamma_{30} d_3)\right) \\ +jk_4^2\gamma_{30} \left[k_2^2\gamma_{30} \cos(\gamma_{20} d_2)\sin(\gamma_{30} d_3) + k_3^2\gamma_{20} \sin(\gamma_{20} d_2)\cos(\gamma_{30} d_3)\right] \end{array} \right] \end{array} \right\} \quad \text{(A9)}$$

$$K_{2,(vv)} = \frac{2jk_1^2k_2^2\gamma_{10}\gamma_{20}\gamma_2(k_2^2 - k_3^2)}{r_v(\gamma_0) r_v(\gamma)} \left\{ \begin{array}{l} \left[\begin{array}{l} k_3^2\gamma_3\gamma_{30} \left(k_4^4\chi\chi_0 - k_2^2k_3^2\gamma_4\gamma_{40}\cos(\varphi - \varphi_0)\right)\cos(\gamma_3 d_3)\cos(\gamma_{30} d_3) \\ -\left(k_3^6\gamma_4\gamma_{40}\chi\chi_0 - k_2^2k_4^4\gamma_3^2\gamma_{30}^2\cos(\varphi - \varphi_0)\right)\sin(\gamma_3 d_3)\sin(\gamma_{30} d_3) \end{array} \right] \\ +jk_3^2k_4^2 \left[\begin{array}{l} \gamma_{30} \left(k_3^2\gamma_4\chi\chi_0 - k_2^2\gamma_{40}\gamma_3^2\cos(\varphi - \varphi_0)\right)\sin(\gamma_3 d_3)\cos(\gamma_{30} d_3) \\ +\gamma_3 \left(k_3^2\gamma_{40}\chi\chi_0 - k_2^2\gamma_4\gamma_{30}^2\cos(\varphi - \varphi_0)\right)\cos(\gamma_3 d_3)\sin(\gamma_{30} d_3) \end{array} \right] \end{array} \right\} \quad \text{(A10)}$$

$$K_{3,(vv)} = \frac{j2\gamma_{10}\gamma_{20}\gamma_{30}\gamma_2\gamma_3 k_1^2k_2^4k_3^2 \left(k_3^2 - k_4^2\right)\left(k_4^2\chi\chi_0 - k_3^2\gamma_4\gamma_{40}\cos(\varphi - \varphi_0)\right)}{r_v(\gamma_0) r_v(\gamma)} \quad \text{(A11)}$$

$$K_{1,(hv)} = \frac{2j(k_1^2 - k_2^2)k_1\gamma_{10}\gamma_{20}\sin(\varphi - \varphi_0)}{r_v(\gamma_0) r_h(\gamma)} \left[\begin{array}{l} k_3^2\gamma_{40} \left(k_2^2\gamma_{30} \cos(\gamma_{20} d_2)\cos(\gamma_{30} d_3) - k_3^2\gamma_{20} \sin(\gamma_{20} d_2)\sin(\gamma_{30} d_3)\right) \\ +jk_4^2\gamma_{30} \left(k_2^2\gamma_{30} \cos(\gamma_{20} d_2)\sin(\gamma_{30} d_3) + k_3^2\gamma_{20} \sin(\gamma_{20} d_2)\cos(\gamma_{30} d_3)\right) \end{array} \right] \times \left[\begin{array}{l} \gamma_3 \left(\gamma_2 \cos(\gamma_2 d_2)\cos(\gamma_3 d_3) - \gamma_3 \sin(\gamma_2 d_2)\sin(\gamma_3 d_3)\right) \\ +j\gamma_4 \left(\gamma_2 \cos(\gamma_2 d_2)\sin(\gamma_3 d_3) + \gamma_3 \sin(\gamma_2 d_2)\cos(\gamma_3 d_3)\right) \end{array} \right] \quad \text{(A12)}$$

$$K_{2,(hv)} = \frac{2j(k_2^2 - k_3^2)k_1k_2^2\gamma_{10}\gamma_{20}\gamma_{30}\gamma_2\sin(\varphi - \varphi_0)}{r_v(\gamma_0) r_h(\gamma)} \left[k_3^2\gamma_{40}\cos(\gamma_{30} d_3) + jk_4^2\gamma_{30}\sin(\gamma_{30} d_3)\right] \times \left[\gamma_3\cos(\gamma_3 d_3) + j\gamma_4\sin(\gamma_3 d_3)\right] \quad \text{(A13)}$$

$$K_{3,(hv)} = \frac{2j(k_3^2 - k_4^2)k_1k_2^2k_3^2\gamma_{10}\gamma_{20}\gamma_{30}\gamma_{40}\gamma_2\gamma_3\sin(\varphi - \varphi_0)}{r_v(\gamma_0) r_h(\gamma)} \quad \text{(A14)}$$

where $\chi = \sqrt{\alpha^2 + \beta^2}$ and $\chi_0 = \sqrt{\alpha_0^2 + \beta_0^2}$.

When $k_2 = k_3 = k_4$ we obtain the first-order SPM Kernels associated with a single rough surface separating two media [2]. When $k_3 = k_4$, we find the first-order SPM Kernels for a stack of two slightly rough interfaces [5]. In addition, we verified that the SPM-kernel values derived from analytical formulas presented in this appendix become identified with those derived from recurrence formulas established in [6].

In the incidence plane (i.e., in the plane $\varphi = \varphi_0$), we find that $K_{i,(hv)} = K_{i,(vh)} = 0$ for $1 \leq i \leq 3$. As a result, in the incidence plane, there is no depolarization and the cross scattering amplitudes $A^{(1)}_{(b\neq a,a)}(\alpha, \beta)$ are equal to zero and the cross-polarized LRSI $S_{(ba,aa)}$ is equal to zero.

In the perpendicular plane (i.e., in the plane $\varphi = \varphi_0 \pm 90°$), $K_{i,(hh)} = 0$ and $K_{i,(vh)} \neq 0$. As a result, under a horizontal polarized incidence, the scattering amplitude $A^{(1)}_{(hh)}(\alpha, \beta)$ is equal to zero and the cross-polarized LRSI $S_{(vh,hh)}$ equal to the unity. By contrast, $K_{i,(vv)} \neq 0$ and $K_{i,(hv)} \neq 0$. So, we can analyze the stratified medium by means of the PDF of random variable $S_{(hv,vv)} = I_{hv}/(I_{hv} + I_{vv})$.

REFERENCES

1. Afifi, S. and R. Dusséaux, "The co- and cross-polarized scattered intensity ratios for 3D layered structures with randomly rough interfaces," *Journal of Electromagnetic Waves and Applications*, Vol. 33, No. 7, 811–827, 2019.
2. Afifi, S. and M. Diaf, "Scattering by random rough surfaces: Study of direct and inverse problem," *Opt. Commun.*, Vol. 265, 11–17, 2006.
3. Tabatabaeenejad, A. and M. Moghaddam, "Bistatic scattering from three-dimensional layered rough surfaces," *IEEE Trans. Geosci. Remote Sens.*, Vol. 44, No. 8, 2102–2114, 2006.
4. Imperatore, P., A. Iodice, and D. Riccio, "Electromagnetic wave scattering from layered structures with an arbitrary number of rough interfaces," *IEEE Trans. Geosc. Remote Sens.*, Vol. 47, No. 4, 1056–1072, 2009.
5. Afifi, S. and R. Dusséaux, "Scattering by anisotropic rough layered 2D interfaces," *IEEE Trans. Antennas Propag.*, Vol. 60, No. 11, 5315–5328, 2012.
6. Afifi, S., R. Dusséaux, and A. Berrouk, "Electromagnetic wave scattering from 3D layered structures with randomly rough interfaces: Analysis with the small perturbation method and the small slope approximation," *IEEE Trans. Antennas Propag.*, Vol. 62, No. 10, 5200–5208, 2014.
7. Dusséaux, R., S. Afifi, and M. Dechambre, "Scattering properties of a stratified air/snow/sea ice medium. Small slope approximation," *Comptes Rendus Physique*, Vol. 17, No. 9, 995–1002, Elsevier Masson, 2016.
8. Afifi, S. and R. Dusséaux, "On the co-polarized scattered intensity ratio of rough layered surfaces: The probability law derived from the small perturbation method," *IEEE Trans. Antennas Propag.*, Vol. 60, No. 4, 2133–2138, 2012.
9. Afifi, S. and R. Dusséaux, "On the co-polarized phase difference of rough layered surfaces: Formulas derived from the small perturbation method," *IEEE Trans. Antennas Propag.*, Vol. 59, No. 7, 2607–2618, 2011.
10. Lee, J. S., K. W. Hoppel, S. A. Mango, and A. R. Miller, "Intensity and phase statistics of multilook polarimetric and interferometric SAR imagery," *IEEE Trans. Geosc. Remote Sens.*, Vol. 32, No. 5, 1017–1028, 1994.
11. Lee, J.-S. and E. Pottier, *Polarimetric Radar Imaging: From Basics to Applications*, CRC Press, Boca Raton, FL, USA, 2009.
12. Mishra, P. and D. Singh, "Role of polarimetric indices based on statistical measures to identify various land cover classes in ALOS PALSAR data," *Proc. APSAR*, 1–4, Seoul, Korea, 2011.
13. Mishra, P. and D. Singh, "A statistical-measure-based adaptive land cover classification algorithm by efficient utilization of polarimetric SAR observables," *IEEE Trans. Geosc. Remote Sens.*, Vol. 52, No. 5, 2889–2900, 2014.
14. Pope, K. O., J. M. Rey-Benayas, and J. F. Paris, "Radar remote sensing of forest and wetland ecosystems in the central American tropics," *Remote Sens. Environ.*, Vol. 48, 205–219, 1994.
15. Da Silva Ramos Vieira Martins, F., J. R. dos Santos, L. S. Galvão, and H. A. M. Xaud, "Sensitivity of ALOS/PALSAR imagery to forest degradation by fire in northern Amazon," *Int. J. Appl. Earth Obs. Geoinf.*, Vol. 49, 163–174, 2016.